Journal of Molecular Liquids 366 (2022) 120269

Contents lists available at ScienceDirect

Journal of Molecular Liquids

journal homepage: www.elsevier.com/locate/molliq

Electric field as a useful tool to improve the poor adsorption affinity of pollutants on carbonaceous aerogel pellets

A. Puga, J. Meijide, M. Pazos, E. Rosales, M.A. Sanromán *

CINTECX, University of Vigo, BIOSUV Group, Department of Chemical Engineering, Campus Lagoas-Marcosende 36310, Vigo, Spain

ARTICLE INFO

Article history:
Received 11 July 2022
Revised 17 August 2022
Accepted 31 August 2022
Available online 13 September 2022

Keywords:
Adsorption
Carbonaceous aerogel pellets
Antipyrine
Sulfamethizole
Fluoxetine
Electrosorption

ABSTRACT

The removal of ionisable drugs (fluoxetine, sulfamethizole and antipyrine) from aqueous solution was performed by conventional adsorption using carbonaceous aerogel pellets as adsorbents. Although >96 % elimination was achieved for sulfamethizole and antipyrine after 1440 min, only 2.5 % fluoxetine was removed. In a multicomponent system, the presence of these three drugs in the solution leads to a fivefold depletion of the adsorbed total mass. Thus, the authors proposed to influence the traditional adsorption process by an electric field to improve the low affinity of fluoxetine to the aerogel. Specifically, the electrosorptive removal of fluoxetine was investigated by applying different voltages between 0.8 and 1.3 V, with the maximum adsorption achieved at 1.2 V. The application of an electric field increases the affinity of the contaminants to aerogel pellets. After demonstrating the applicability of the electrosorption in the removal of fluoxetine, the effect of the water matrix on the process was analysed. For this purpose, the removal of these ionisable drugs was evaluated using real wastewater, specifically, raw wastewater and wastewater after primary and tertiary treatment from a municipal wastewater treatment plant. As expected, pollutant removal was somewhat lower due to the complexity of the water matrix. Total percent removal of all pollutants was achieved using only the effluent treated water as the matrix due to minimal competitive adsorption. Finally, the Microtox® test confirmed the excellent ability of this approach to remove these pharmaceuticals, resulting in luminescence inhibition that decreased by 60–80 % depending on the water matrix compared to the polluted influent.

1. Introduction

The widespread use of pharmaceuticals, particularly antibiotics, saved millions of lives in the 20th century by providing appropriate treatment against pathogens and microorganisms [20,16]. The consumption of human and veterinary medicines has increased in recent decades due to the growing global population and their life expectancy in many developed countries, increasing investment in healthcare, and advances in research and development [15]. The market has grown considerably since 2017; specifically, global pharmaceutical sales were $1.14 trillion and are expected to reach $1.46 trillion in 2021 [15]. North America accounts for the majority of this data due to the remarkable U.S. pharmaceutical industry. It is well known that the pharmaceutical compounds are non-biodegradable, affecting ecological imbalance and biological functions [19]. In addition, these organic compounds and even, their metabolites have been detected at trace levels (ranging from ng/L to mg/L) in surface waters, wastewater, sediments, groundwater, and drinking water. Their toxic and recalcitrant properties hinder their complete removal by biological processes. Therefore, the application of other technologies in the field of water treatment, especially in the pharmaceutical effluents, has attracted much attention to reduce the input of these pollutants into aquatic ecosystems via wastewater [51]. Among others, adsorption allows the removal of pollutants from the main solution without producing toxic by-products [27].

Several researchers have reported the removal of ionisable drugs using carbon-based materials such as activated carbon, biochar, carbon nanotubes, graphene oxide, or carbon felt [2]. As is well known, electrostatic interactions play a predominant role in adsorption processes using carbon-based materials [21], usually controlled by the pH of the solution, due to the dual contribution of the dissociated forms of the pollutants and the surface chemistry of the adsorbents. Thus, electrosorption is considered a suitable alternative for the removal of ionisable drugs from aqueous solutions. This technology is a non-Faraday process in which the electrochemical polarisation of the electrodes increases the adsorption capacity [10,54]. The use of a three-dimensional electrode (3D) system provides an excellent approach for wastewater treatment,

* Corresponding author.
E-mail address: sanroman@uvigo.es (M.A. Sanromán).

https://doi.org/10.1016/j.molliq.2022.120269
0167-7322/

allowing a larger electroactive surface area and a shorter distance for mass transfer [61]. Direct polarisation of carbonaceous materials at high potentials can lead to their attrition and reduce the effectiveness of the process. With a sufficiently applied electric field, conductive particles can be polarised by the movement of electric charge, leading to the formation of multiple-charge microelectrodes, with an anodic and a cathodic side [34]. Therefore, the charged particles can trigger the electroadsorption process and even the electrolytic degradation of the adsorbed compounds. Moreover, the adsorbent can be *in-situ* regenerated by switching off the electric field or even changing the polarity of the electrodes, which prolongs the half-life and reduces the operating cost [11]. Similarly, the *in-situ* regeneration of the saturated carbon electrodes could be achieved by a subsequent degradation process using electro-Fenton or electro-peroxone treatment [12,18].

Although electrochemical-based techniques have been successfully used for the removal of pharmaceuticals [29], few works have analysed the electrosorption / electrodesorption capacity of carbonaceous materials for the removal of pharmaceuticals and personal care products [11,54,57,58]. The removal of three ionisable antibiotics (sulfadimethoxine, ciprofloxacin, and clarithromycin) on an activated carbon fiber as a cathodic electrode was tested by Wang et al. [54]. The authors reported that the concentration of the effluent decreased from > 100 μg/L to 9.6 μg/L at fixed potential (1.0 V). In the same way, Tang et al. [50] tested Fe_3O_4 nanoparticles as a 3D electrode with peroxydisulphate to enhance the degradation of tetracycline by electroadsorption followed by electrooxidation. Under optimised experimental conditions, around 85 % were removed after 60 min. Recently, Sanroman's group analysed the application of a carbonaceous aerogel honeycomb monolith to remove diclofenac from water by electroreversible adsorption [41]. The total regeneration of the aerogel was carried out by cathodic polarization, which allowed the reusability of the adsorbent in three successive electrosorption/electrodesorption cycles. Its 3D structure promotes mass transfer and improves the hydrodynamic conditions in the electrochemical system [42]. In recent years, aerogels have attracted attention of material scientists. Aerogels are materials that have low density, high surface area, and large pore volumes [5]. Moreover, its large surface area and pore volume play an important role as capacitive electrodes for adsorption of ions from the electrolytic solution. This reversible option offers remarkable advantages for wastewater treatment even at low pollutant concentrations.

All these considerations motivated the present work to investigate the ability of an electrosorption strategy to remove ionisable pharmaceuticals from an aqueous solution using an aerogel. Three common pharmaceuticals (fluoxetine, sulfamethizole and antipyrine) were used as model drugs for the conventional adsorption process. In addition, the electrosorptive removal of fluoxetine was investigated using different potentials and water matrices. Then, the performance of a ternary system using municipal wastewater spiked with these three pollutants was evaluated. All experimental data were matched with empirical kinetic models and isotherms to estimate model parameters. Finally, a toxicological analysis was performed using the Microtox® test to evaluate the effectiveness of the process.

2. Materials and methods

2.1. Reagents and aerogel

Antipyrine (>97.5 % purity), sulfamethizole (>99 % purity) and fluoxetine (>99.9 % purity) purchased from Sigma-Aldrich were evaluated as target pollutants and their main characteristics are described in Table S1. All initial solutions were prepared using Milli-Q grade water as solvent. Real wastewater samples were collected from raw wastewater and effluents after primary and tertiary treatment in a municipal wastewater plant (Guillarei, Spain). Their physicochemical properties are summarised in Table S2. The carbonaceous aerogel pellets were prepared by sol-gel polycondensation of resorcinol, melamine, and formaldehyde mixtures followed by supercritical drying to obtain their pore structure. They were immersed in an acetone solution containing $Fe(NO_3)_2{\cdot}9H_2O$ to add iron nanoparticles to the aerogel structures during the synthesis process [60].

2.2. Structural characterisation of the aerogel

The crystallinity of the aerogel samples was investigated by X-ray diffraction (XRD) on a Siemens D5000 diffractometer (Bruker AXS Gmbh, Karlsruhe, Germany) using a copper anode and a graphite monochromator to generate CuKα radiation (λ = 0.154 nm), at 40 kV voltage and 40 mA current. The XRD patterns were scanned by using 2θ angle from 5° to 80° at 0.026°/s scan rate (CACTI, University of Vigo). The average crystallite size of the aerogel was estimated using Scherrer's equation (Eq. (1)) [36].

$$D = 0.89\,\lambda / (\beta \cdot \cos\,\theta_B) \quad (1)$$

where D is the average crystallite size (nm), λ is the wavelength of the X-ray radiation (nm), β is the full-width at half-maximum intensity (FWHM) and θ_B is the half diffraction angle (rad). The basal spacing was determined by the Bragg's law (Eq. (2)).

$$d = \lambda/2\sin\theta \quad (2)$$

where d is the basal spacing (nm), λ is the wavelength of the X-ray radiation (nm) and θ is the diffraction angle (rad).

The nature of the synthesised aerogel was determined by Raman spectrometry. Spectra were recorded at room temperature on the Horiba Jobin-Yvon HR800 LabRAM system using a He-Ne laser at an excitation wavelength of 632.8 nm and 20 mW power. An optical microscope with a 100× objective lens was used to focus the laser beam on the samples and collect the scattered radiation (CACTI, University of Vigo). The surface functional groups were studied by Fourier transform IR (FTIR) spectra using Nicolet 6700 FT-IR spectrometers (Thermo Electron Corporation) in the range 4000–400 cm^{-1} with a resolution of 4 cm^{-1} and 32 scans (CACTI, University of Vigo). The spectra of the samples were recorded in KBr pellets containing 1 wt % of the material. Prior the KBr pellets preparation, all samples and KBr were oven dried overnight at 100 °C. Finally, the thermal properties of this material were studied by thermogravimetric analysis (TGA) using TG-DSC SETSYS Evolution 16/18 (Setaram, Caluire, France). The aerogels were heated at 10 °C/min up to 800 °C under inert nitrogen flow (CACTI, University of Vigo).

2.3. Nanotextural and chemical characterisation of the aerogel

The nanotexture of the aerogels was characterised by measuring the nitrogen adsorption isotherms at 196 °C (ASAP 2020 Plus, Micromeritics). Before experiments, the samples were degassed under vacuum conditions (10 mmHg) at 200 °C overnight (SAI, University of A Coruña). Isotherms were used to determine BET surface area, total pore volume and pore size (d_P). BET surface area before and after the electrosorption was estimated using the Brunauer-Emmett-Teller equation. Total pore volume was calculated from the adsorption volume at a relative pressure of ~ 0.995 (corresponding to a pore size of ~ 85 nm). The micropore volume was estimated from the Dubinin-Radushkevich plot and the mesopore volume was determined by the difference compared to the total volume [6]. The morphological characteristics of these aerogels were observed under the field emission scanning

electron microscope and energy-dispersive X-ray spectroscopy (FE-SEM/EDS) on the JEOL JSM 6700F (Japan) equipped with an energy dispersive X-ray spectrometer (EDS) using an accelerating voltage of 20 kV (CACTI, University of Vigo). The point of zero charge of these aerogels (pH_{PZC}) was estimated using a mass titration method as described elsewhere [45]. Furthermore, the content of the oxygenated functional groups on the aerogel surface was determined by Boehm titration procedure [8,14].

2.4. Experimental setup

The adsorption kinetics of these target pollutants were tested using a pellet-liquid ratio of 0.1 mg/20 mL and the experiments were conducted in a 50 mL undivided cylindrical glass vessel. For the electrosorption studies, the aerogel pellets were placed in the centre of the glass vessel, while upright carbon felt electrodes (Mersen, RVG-2000), with 99.9 % carbon content, 0.088 g/cm^3 density and 0.7 m^2/g surface area (2.5 × 1.0 × 0.5 cm) were placed 1.5 cm apart between the electrodes. Both electrodes were immersed in the main solution (20 mL pharmaceutical target solution at natural pH) at room temperature under magnetic stirring to avoid concentration gradients. Electrochemical measurements at different voltages (0.8, 1.0, 1.2 and 1.3 V) were performed using the AUTOLAB Potentiostat/Galvanostat (AUTOLAB PGSTAT 30 Metrohm). Duplicate experiments were performed and concentrations are the average of triplicate analysis (standard deviation<5 %).

2.5. Analytical methods

2.5.1. Chromatographic conditions

The decays of antipyrine and sulfamethizole were monitored by HPLC (Agilent 1100) equipped with a Zorbax Eclipse XDB-C8 reverse column (150 × 4.6 mm i.d. 5 μm). The injection volume was set at 10 μL and the mobile phase, a mixture of acetic acid: water: acetonitrile (1.5:87.5:10 v/v/v) was pumped by isocratic elution. For fluoxetine analysis, Poroshell 120 column (4.6 × 50 m m 2.7 μm) was used as stationary phase, 5 μL as injection volume and the mobile phase consisting of acetonitrile: water: phosphoric acid (10:89.9:0.1 v/v/v) was pumped in gradient mode (from 10 % to 100 % acetonitrile after 5.5 min and then, re-equilibration). Before chromatographic analysis, all samples were filtered through 0.45 μm PVDF filters. The column was kept at room temperature for antipyrine and sulfamethizole, while the fluoxetine analysis was performed at 40 °C. Detection was performed using a diode array detector at 228 nm (fluoxetine), 242 nm (antipyrine) and 274 nm (sulfamethizole). Identification and further quantification of the analytes was performed by comparing of the retention time and the area under the peak, respectively.

2.5.2. Inorganic ion concentration

The concentration of nitrite, nitrate and phosphate ions was determined by ion chromatography (Dionex ICS-3000) coupled with an anionic exchange column, Metrosep A Supp 5 250/4.0 mm. The injection volume was 20 μL and the mobile phase, consisting of 3.2 mM sodium carbonate and 1.0 mM sodium hydrogen carbonate solution, was pumped at 0.7 mL/min (CACTI, University of Vigo).

2.5.3. Chemical oxygen demand determination

Chemical oxygen demand (COD) decay was measured using a UV-spectrophotometer (DR-2800, Hach Lange; Germany) with LCK 514 cuvette tests according to the official protocol standards DIN 38409-H41-H44 and ISO 6060-1989. For this purpose, a strong oxidizing agent such as sulphuric acid-potassium dichromate solution was used in the presence of a silver sulfate catalyst for the quantification of oxidizable organic compounds by the reduction of dichromate ions ($Cr_2O_7^{2-}$) to green chromium ions (Cr^{3+}). After the oxidation step, the green coloration of Cr^{3+} was measured photometrically.

2.6. Energy consumption

The viability of the electrosorption process for industrial applications was evaluated based on the energetic parameters [30]. With constant applied potential, the energy consumption per unit mass (EC) can be analysed using Eq.3.

$$EC\,(kWh/kg) = 1000 \cdot E_{cell} \cdot I \cdot t / (\Delta C \cdot V) \quad (3)$$

where E_{cell} is the average potential difference of the cell (V), I is the applied current intensity (A), ΔC is the adsorbed pollutant concentration (mg/L), V is the volume (L) and t is the electrolysis time (h).

2.7. Toxicity assessment

The Microtox® standard test is based on the quantification of light emission from a marine bacterium in the presence of toxicants. The lyophilized Microtox reagent (*Vibrio fischeri*) and solutions were obtained from Drogallega (Spain). Acute toxicity testing was performed using an 81.9 % screening test protocol in which the marine bacterium was exposed to a range of serial dilutions ranging from 0 to 81.9 % (geometric factor = 2). After 5- and 15-min exposures to each aqueous solution, bacterial bioluminescent emission was measured and compared to a control sample using Microtox® Omni™ software version 4.3.0.1.

3. Results and discussion

3.1. Structural characterisation of the carbonaceous aerogel pellets

The structural properties of these materials were analysed by XRD, Raman spectroscopy, FTIR and TGA. As can be seen in Fig. 1a, the XRD patterns of the aerogels are characterized by two broadened bands at approximately 26° and 44° (2θ), which are assigned to (002) and (100) reflections, respectively. The XRD patterns are characteristic of the disordered carbon annealed at low temperature (below 1000 °C). These results are in agreement with those of Zafra et al. [60], who had previously analysed the XRD profile of the raw materials. Moreover, the iron incorporation showed additional peaks assigned to the (020) and (110) reflections of goethite (JCPDS 00-017-0536) and maghemite corresponding to the (311), (400) and (511) reflections (JCPDS 00-039-1346). Further information about the structure of the aerogel was obtained by Raman spectroscopy (Fig. 1b). The Raman spectrum showed two distinguishable peaks, the G band at ~ 1580 cm^{-1} and the D band at ~ 1350 cm^{-1}, which were attributted to the vibrations of the sp^2-bonding carbon atoms in the 2-dimensional hexagonal lattices and the defects, respectively. The intensity ratio of the D-band to the G-band ($I_D'I_G$) determined in the deconvolution of the Raman bands allows the evaluation of the lattice disorder of the carbon-based materials and thus, the graphitic nature of these samples [37,39]. The samples exhibited a slightly lower ratio (around 1.20), confirming a partially ordered structure. A higher degree of graphitization is associated with the existence of an amorphous carbon phase, suggesting excellent adsorption properties [56]. These results are consistent with previous conclusions from the XRD pattern [28]. From $I_D'I_G$ ratio, the average size of sp^2 carbon atoms in the plane associated with electrical conductivity can be estimated using Eq. (4).

$$L_a = 2.4 \cdot 10^{-10} \cdot (\lambda_l)^4 / (I_D/I_G) \quad (4)$$

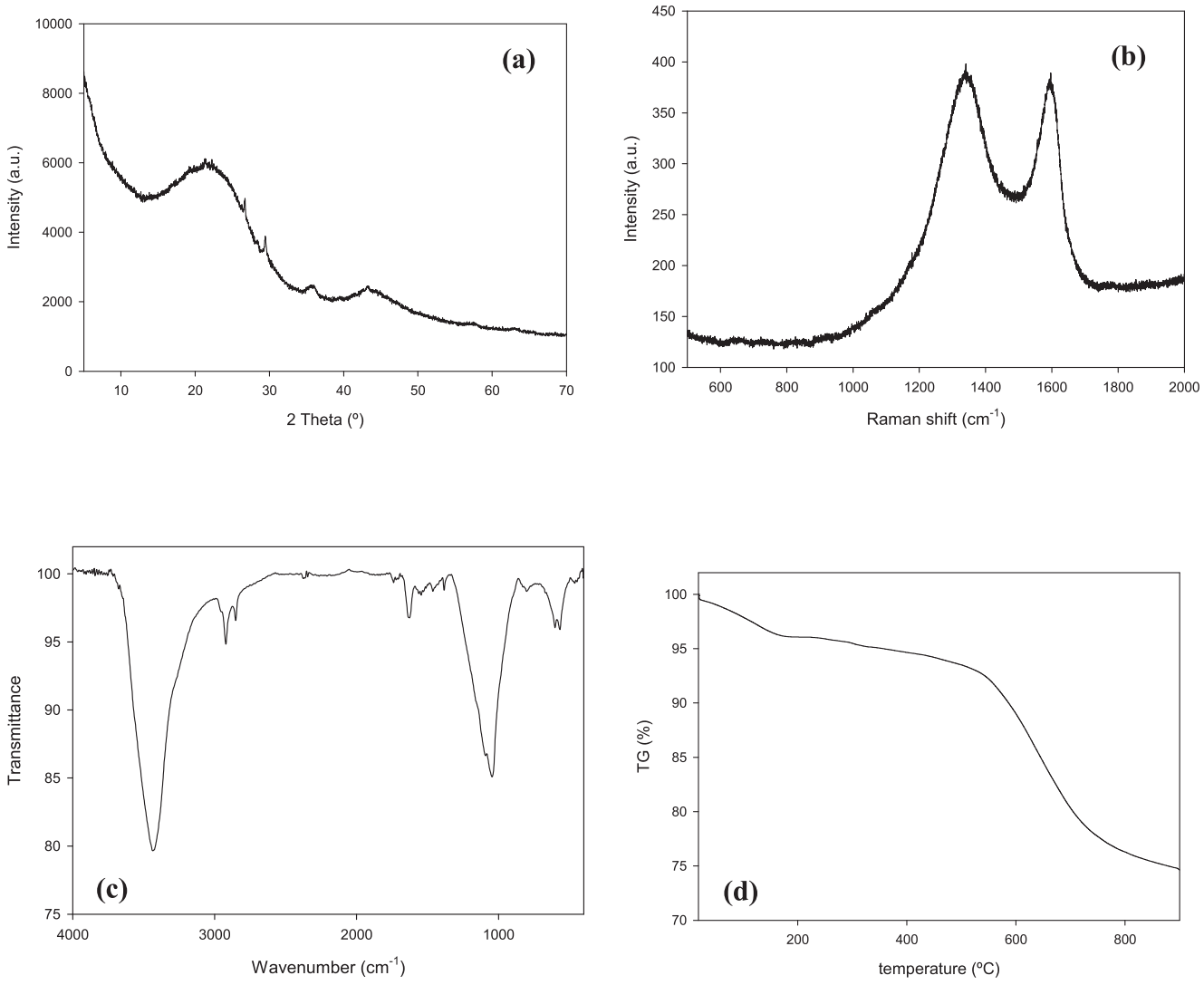

Fig. 1. Characterization of raw aerogel: (a) XRD spectrum, (b) Raman spectrum, (c) FTIR spectra, (d) TGA profile.

where λ_l is the wavelength of the input laser line (632.8 nm). Based on the I_D/I_G ratio, the L_a value was 33.46 nm for the raw aerogels. Thus, the materials have considerable defect density, which negatively affects their electrochemical performance, while the higher size of the in-plane sp^2 carbon atoms improves their electrical conductivity.

As shown in Fig. 1c, FTIR analysis was used to detect the presence of functional groups and chemical bonds from the synthesis process. The FTIR spectra show the characteristic bands of the O—H and N—H stretching vibrations at 3500 cm^{-1}, the C—H stretching vibration around 2900 cm^{-1} and the peak around 1700 cm^{-1} corresponding to the stretching vibrations of C=O and C=C. Moreover, the intense band in the fingerprint region corresponds to the C—O stretching vibration at 1100 cm^{-1}. The bands in the 1465–1380 cm^{-1} region correspond to the bending vibration of the C—H bond and the bending vibration of the O—H bond at 1630 cm^{-1}. The presence of iron was confirmed by the characteristic band at 600 cm^{-1} associated with the Fe—O stretching vibrations of the magnetite lattice. Many authors reported the incorporation of nitrogen atoms from the melamine precursor into the graphitic network [44]. The chemical reactions between the —NH groups present on the aerogel surface and the drug structure may indeed contribute to the adsorption of the organic compounds.

The presence of multiple functional groups on the aerogel surface was also demonstrated by TGA under nitrogen atmosphere (Fig. 1d). A negligible effect attributed to iron was found. The obtained curves are similar to those previously reported in the literature for resorcinol-formaldehyde-melamine-based aerogels without iron particles [44,53]. The release of the organic precursors, mainly formaldehyde, and water removal at the aerogel surface lead to mass loss at temperatures below 150 °C. The water adsorbed in the deepest pores and the degradation of methyl, hydroxyl, and amine-groups lead to the release of the volatile compounds. Nonetheless, the sharp peak detected at 350 °C indicates the decomposition of all the basic organic compounds (formaldehyde, melamine and ammonium) [59]. In addition, charring of the samples at above 600 °C resulted in a higher percentage of mass loss due to the breaking of C—H bonds. Note that the reduction of some iron-containing species present in the aerogel structure may also contribute to the mass loss observed in the TGA analysis. These processes are iron- dihydroxylation

(goethite → maghemite), iron reduction (maghemite → ferrous oxide) and then, complete reduction to iron metal, which take place at 420, 600 and 900 °C, respectively [4].

3.2. Nanotextural and chemical characterisation of the aerogels

The nanotextural properties of the aerogels were monitored by measuring the nitrogen adsorption-desorption isotherms at −196 °C. They were used to estimate the total, meso and micropore volume and BET surface area from the nitrogen adsorption-desorption measurements. These materials exhibit high porosity and apparent specific surface area due to the compact structure of melamine and subsequent supercritical drying [62]. All textural parameters determined using the nitrogen isotherm are summarized in Table 1. In addition, all samples exhibited a type IV isotherm pattern, the characteristic feature of mesoporous solids with pore sizes ranging from 2 to 50 nm according to the IUPAC classification [52]. The observed hysteresis loop was attributed to capillary condensation that occurred in the mesopores, while the shape and position of the loop depended on the morphology of the solid (specific pore structures and even, the degree of compaction). The morphology of the samples was analysed at SEM and shows a typical open-pore 3-D particle network. As can be seen in Fig. 2a, the SEM image shows a smooth compact surface resulting from the compaction of the structure of packed spherical particles. An identical structure was previously reported by Muehlemann et al., [31], who prepared a resorcinol-melamine-formaldehyde based carbon xerogel. The elemental composition of aerogels was investigated using the EDS spectrum (Fig. 2a). High levels of carbon and oxygen were detected and, to a lesser extend, some metals such as iron and copper were detected, confirming the expected chemical composition. The traces of sodium correspond to the residues of the sodium carbonate catalyst used in the SEM sample preparation. The chemical composition, previously determined by XRD and FTIR analyses was consistent with the EDS spectrum.

Carbon-based materials have an amphoteric character and their behaviour is therefore strongly dependent on the pH of the solution. Consequently, the effect of pH on surface charges was quantified by pH_{PZC} determination over a wide pH range (3.5–10.5). From their results, the authors concluded that the pH_{PZC} corresponds to a circumneutral pH (around 7.3), as shown in Fig. S1. The material surface is positively charged at a pH below the pHPZC, which promotes the adsorption of anionic species, while a negative charge at a pH above pH_{PZC} favors the adsorption of cationic species [13]. Moreover, the functional groups on the adsorbent surface were determined by Boehm titration by selective neutralization using base solutions of increasing strength [8]. According to Boehm, NaOH neutralizes all acidic groups (carboxyl, phenolic and lactone groups), Na_2CO_3 (pK_b = 3.8) neutralizes carboxyl and lactone groups, while $NaHCO_3$ (pK_b = 7.6) neutralizes only carboxyl groups. The phenolic groups account for about 55.5 % of the acidic group content, which is due to the use of resorcinol as the main organic precursor, a phenolic monomer with three functional active sites more reactive than phenol. These results are consistent with the FTIR pattern, in which stricking peaks characteristic of phenolic structures can be seen, including two bands around 800 and 1100 cm^{-1} assigned to C=C bending for alkenes (flavonoids) and C—H stretching vibration for phenols, respectively [1].

3.3. Adsorption process of target pollutants

The adsorption of three individual drugs (antipyrine, sulfamethizole, and fluoxetine) was evaluated on the characterised aerogel pellets. Literature indicates that adsoprtion can occur through pore filling, hydrophobic interactions, partitioning, hydrogen bonding, π-π or electrostatic interactions [40,49].

At natural pH values ranging from 4 to 6, the surface of the aerogel is positively charged, while the sulfamethizole and antipyrine are predominantly in neutral form. These facts confirm that electrostatic interactions are not the main mechanism for the adsorption process, suggesting the presence of hydrophobic and π-π interactions [55]. Incidentally, fluoxetine at pH 6 has a higher proportion of cationic species and therefore, a negligible percentage of removal was observed at these experimental conditions due to the repulsive electrostatic interactions. The pH-dependent speciation of each pollutant is shown in Fig. S2. Furthermore, the equilibrium adsorption capacity values of sulfamethizole and antipyrine (Table 2), expressed in μmol/g showed a linear relationship with their pH-dependent octanol-water partition coefficient (log D) at natural pH. This fact is probably due to the presence of hydrophobic interactions, which are considered to be the crucial phenomena for the adsorption of organic pollutants by carbon-based materials [23,24,48]. The well-known empirical pseudo-first and pseudo-second kinetic models were used to fit the experimental data to elucidate the control mechanism of pharmaceutical adsorption. The estimated kinetic parameters are summarized in Table 2. The experimental data of antipyrine adsorption on the aerogel surface were accurately described by the pseudo-first order kinetic model, indicating that the physisorption process plays a significant role in the process. In contrast, the adsorption of sulfamethizole was described by a pseudo-second order model, confirming that the chemisorption is the main mechanism of the adsorption process. These results are in agreeemt with those of Serna-Carrizales et al. [47], who tested the adsorption of three sulfonamides on activated carbon. For the adsorption of fluoxetine, no adjustment was made for kinetic analysis due to the negligible removal percentage (∼2.5 %).

For a multicomponent system, the presence of additional pharmaceuticals in the solution leads to a greater depletion of the total adsorbed amount of all drugs. More specifically, around 20 % removal was achieved for antipyrine and sulfamethizole after 600 min, while the fluoxetine depletion is considered practically negligible (∼1.2 %). The competitive equilibrium adsorption capacity for antipyrine and sulfamethizole, expressed in μmol/g was consistent with log D values [48]. Similar behaviour was explained by Nielsen and Bandosz [33], who analysed the competitive adsorption of pharmaceuticals (carbamazepine, sulfamethoxazole and trimethoprim) on waste-based materials. The competition of

Table 1
Structural and nanotextural properties of the raw and after electrosorption of commercial aerogel.

Sample	Lattice disorder[a]		Surface area[b] (m^2/g)	Pore volume[b] (cm^3/g)	Average pore diameter[b] (Å)
	I_D/I_G	L_a (nm)			
Raw aerogel pellets	1.15	33.46	385.64	0.179	18.53
Aerogel pellets after electrosorption	1.21	31.80	472.27	0.195	16.54

[a] Estimation by Raman spectrum.
[b] Estimation by BET analysis.

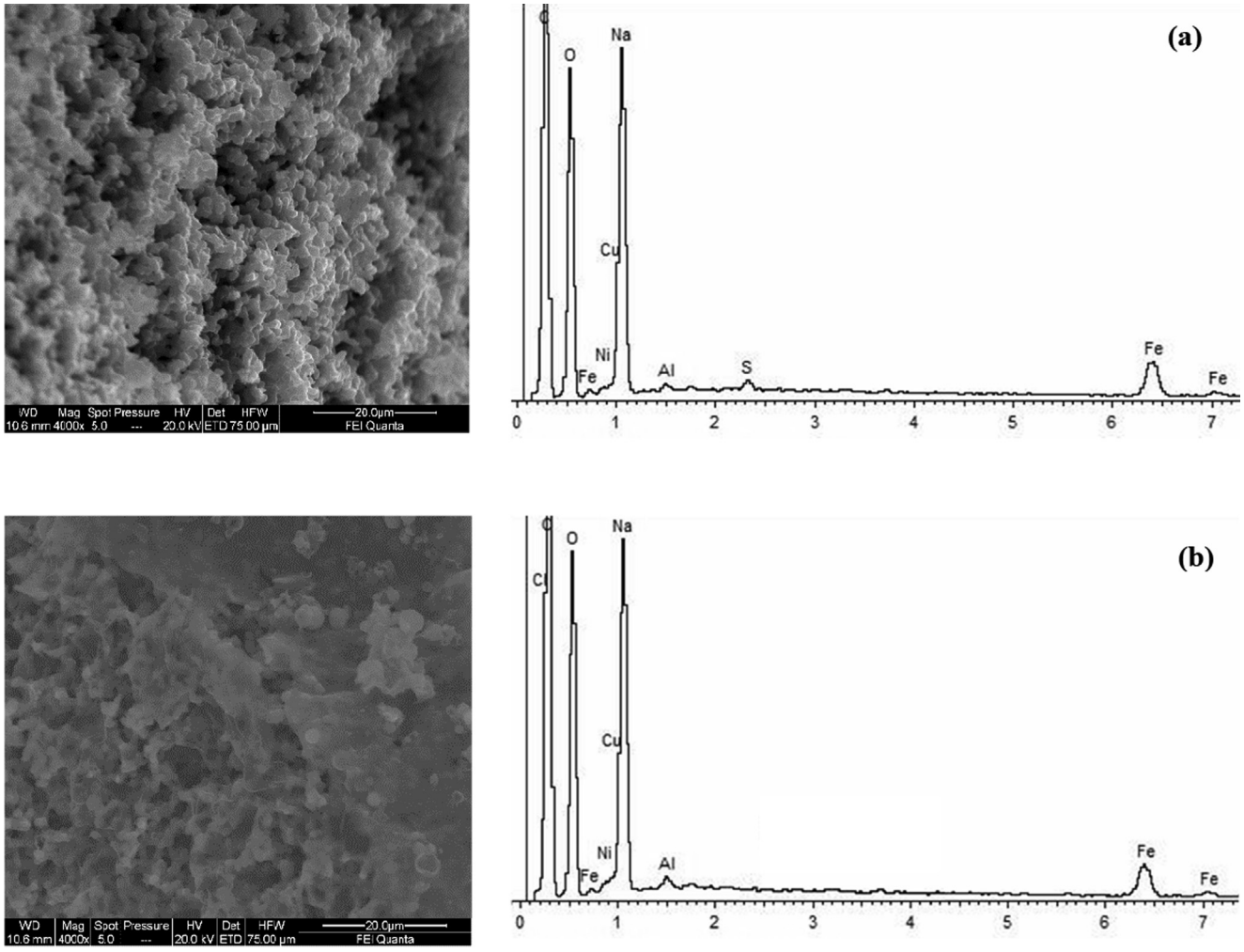

Fig. 2. SEM micrographs and the elemental composition from EDS results of: a) raw aerogel and b) after electrosorption.

Table 2
Pseudo-first and pseudo-second order kinetic parameters for antipyrine and sulfamethizole removal on single and multicomponent system. Conditions: $[Pollutant]_0$ = 10 mg/L, pellet-liquid ratio = 0.1 mg/ 20 mL, natural pH, t = 1440 min.

Operation conditions	Pollutant	$q_{e,\ exp}$ (mg/g)	Pseudo-first order $q_t = q_e\ (1- \exp\ (-k_1 \cdot t))$				Pseudo-second order $q_t = t/((1/k_2 \cdot q_e^2)+(1/q_e) \cdot t)$			
			q_e (mg/g)	k_1 (min^{-1})	R^2	SEE	q_e (mg/g)	k_2 (g/mg·min)	R^2	SEE
Single system	**Antipyrine**	2.000	2.013	0.005	0.997	0.044	2.263	$2.87 \cdot 10^{-3}$	0.983	0.110
	Sulfamethizole	1.840	1.811	0.006	0.990	0.071	1.993	$4.30 \cdot 10^{-3}$	0.999	0.006
Multicomponent system	**Antipyrine**	0.392	0.410	0.005	0.994	0.013	0.524	$8.41 \cdot 10^{-3}$	0.994	0.013
	Sulfamethizole	0.383	0.397	0.005	0.993	0.013	0.503	$9.25 \cdot 10^{-3}$	0.994	0.012

available adsorption sites has a remarkable negative effect on the pollutant adsorption, which shows around 80 % removal decay.

Competitive adsorption of these pharmaceuticals was studied using pseudo-first and pseudo-second order kinetic models under optimized conditions. These results are listed in Table 2; nevertheless, since no clear conclusions could be drawn about the adsorption mechanism, internal diffusion kinetic models were used to fit the obtained results. The effect of intraparticle diffusion was evaluated by fitting the experimental data set to Eq. (5).

$$q_t = k_{id} \cdot t^{0.5} + I \quad (5)$$

where q_t is the adsorption capacity at time t (mg/g), k_{id} is the intraparticle diffusion rate constant (mg·g/ $min^{0.5}$) and I is the intercept (mg/g).

In the intraparticle diffusion model (Fig. S3), no multilinearity of the adsorption process and a near-zero intercept were detected, so intraparticle diffusion can be considered a rate-limiting step. The diffusion coefficient for the adsorption of pharmaceuticals on the aerogel can be calculated using Eq. (6) [46].

$$D_t = 0.03 \cdot r^2 / t_{1/2} \quad (6)$$

where D_t is the intraparticle diffusion coefficient (cm^2/s), r is the average radius of the aerogel (cm) and $t_{1/2}$ is the time required to reach half adsorption fraction (min). Moreover, the intraparticle diffusion coefficients of 10^{-5} to 10^{-13} cm^2/s allow us to correctly assume that this mechanism corresponds to the rate-limiting phase, especially in chemisorption systems [38].

The results suggest the existence of a mechanism complex and, so the experimental data were fitted to an empirical diffusion-chemisorption kinetic model developed by Chittoo and Sutherland [9]. The non-linear form equation is given by the Eq. (7).

$$q_t = (q_e \cdot K_{CD} \cdot t^n) / (K_{CD} \cdot t^n + q_e) \quad (7)$$

where K_{CD} is the chemisorption diffusion rate constant (mg/g·t^n).

After fitting the experimental data to the Sutherland model, the authors proposed a multi-mechanism reaction, with the process controlled by intraparticle diffusion followed by chemisorption. This fact results from the high coefficients of determination and the low standard error of estimate (SEE), as well as the intraparticle diffusion coefficient estimated by Eq. (6), whose values are around $1.2{\cdot}10^{-5}$ cm^2/s, confirming intraparticle diffusion as the rate-limiting step.

3.4. Electrosorption of fluoxetine

Based on the above, the adsorption of fluoxetine on the aerogel pellets was analysed by electrosorption. Batch experiments were performed using a potentiostat at 0.8, 1.0, 1.2 and 1.3 V under magnetic stirring. The process performance depends on the composition of the feed, the electrode materials, and the applied voltage, which are a driving force in the systems that characterise the thickness of the electrical double layer at the interface between the electrode material and the electrolyte solution [25]. Control runs revealed minimum removal percentages related to adsorption on the carbon felt electrode and oxidation at these applied voltages, which ensures the electrochemical stability of fluoxetine. These results are in agreement with those of Ramos et al. [43], who demonstrated the stability of the fluoxetine at low potentials using glassy carbon and boron-doped diamond as electrodes. To this end, the authors recorded several cyclic voltammograms of the aqueous 0.01 M Na_2SO_4 solution in the presence and absence of the fluoxetine at 20 mV/s scan rate using a potential range between +0.5 and +2.0 V. Both electrodes have a wider potential window in the anodic region, where oxidation of the fluoxetine was detected at around +1.7 V.

The applied current was monitored for each potential and reached relatively constant values up to 1.2 V, confirming slower faradaic reactions. As shown in Fig. 3, the use of 1.3 V as the applied voltage resulted in a slight attenuation of fluoxetine removal, due to the presence of side reactions such as water electrolysis and oxidation of the carbonaceous material. The influence of several variables on the electrosorption makes it difficult to establish a reasonable correlation between the applied voltage and the adsorption capacity. The charge of the electrochemical double layer within the pores (capacitance) depends on the plausible contribution of the slow faradaic reactions on the aerogel surface (pseudocapacitance) and the aerogel surface charge [26]. The presence of an electric field on the 3D electrode system promotes polarisation of the carbonaceous materials, leading to an electrosorption process in an elective active region [22]. The pore volume of the aerogel and the functional groups on the surface are slightly affected by the polarization and thus, the increase of the removal percentage can be attributed to the plausible changes on the charged aerogel surface and/or the ionization of the pollutants. The plausible interactions with negatively charged functional groups on the aerogel surface were discarded in view of the negligible fluoxetine adsorption in the conventional adsorption process. The electrosorption experiments were performed at pH 6.5–7.5 with only the cationic form of fluoxetine present in the bulk solution (Fig. S2c). Therefore, most of the adsorption of fluoxetine species on the pellet surface (negatively charged surface) occurs through electrostatic interactions. To confirm the adsorption mechanism the adsorption isotherms were carried out and the most commonly used isotherm models (Langmuir, Freundlich and Redlich-Peterson) were selected to evaluate the process (Table 3). The good fitting to the Langmuir isotherm for fluoxetine adsorption (R^2 0.997) may suggest that the active sites are equally distributed on the surface and the adsorption occurs in a monolayer, that confirms the previous hypothesis. In this electrosorption process, all binding sites have the same affinity for the adsorbate with no interaction between them. In this case, the b_L parameter, which shows the affinity of adsorbent-adsorbate, with low values (0.0763) indicated a relationship towards physisorption in this process. These behaviour is similar than reported by Narayanan et al. [32], in which the Langmuir isotherm model satisfactorily fitted the adsorption data, showing that the adsorption of fluoxetine involved physical adsorption through intermolecular electrostatic force between the adsorbent and fluoxetine. When a more complex model was considered (Redlich-Peterson model), it can be observed that it presents a limiting behaviour β_{RP} = 1 and, thus, confirming the monolayer adsorption with the model expression be reduced to the Langmuir form.

The FTIR spectrum after adsorption allowed the detection of the characteristic bands of fluoxetine, including the stretching vibration of the amine and halide functional groups at 3106 and 1310 cm^{-1}, respectively (Fig. S4a).

The experimental data were fitted to the pseudo-first and pseudo-second kinetic models to determine the control step in fluoxetine electrosorption. The estimated kinetic parameters are summarised in Table 4. Although the theoretical adsorption capac-

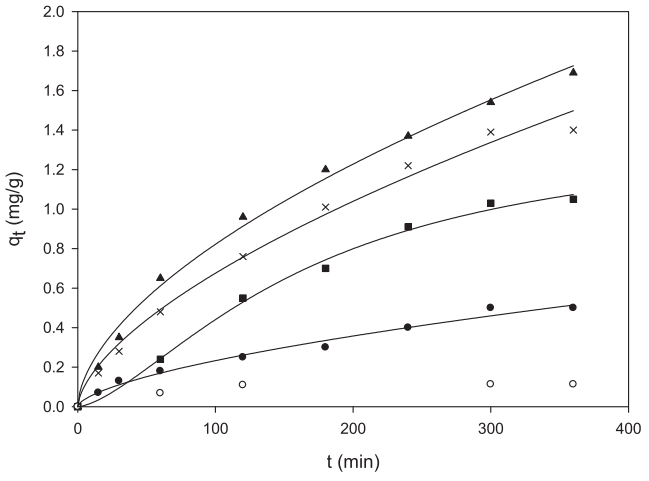

Fig. 3. Effect of the applied voltage on the electrosorption process of fluoxetine. Conditions: $[Fluoxetine]_0$ = 10 mg/L, pellet-liquid ratio = 0.1 mg/ 20 mL, natural pH, V = open-circuit (white circle), 0.8 V (black circle), 1.0 (black square), 1.2. V (black triangle up) and 1.3 V (black thin X). Data represent mean values with a standard deviation below 5 %.

Table 3
Isotherm models and their parameters for fluoxetine electrosorption assays at 1.2 V.

Models	Parameters	
Langmuir	q_{max}(mg/g)	3.66
$q = q_{max} \cdot b_L \cdot C/(1 + b_L \cdot C)$	b_L(L/mg)	0.0763
	R^2	0.9970
Freundlich	K_F ($mg_F^{1-1/n} \cdot L_F^{1/n}$/g)	0.5801
$q = K_F \cdot C_F^{1/n}$	n_F	0.3859
	R^2	0.95979
Redlich-Peterson	K_{RP} (L/g)	0.2796
$q = K_{RP} \cdot C/(1 + a_{RP} \cdot C^{\beta})$	a_{RP} (L/mg) $^{\beta}$	0.0763
	β	1.000
	R^2	0.9970

Table 4
Pseudo-first and pseudo-second order kinetic parameters for fluoxetine on the electrosorption process. Conditions: $[Fluoxetine]_0$ = 10 mg/L, pellet-liquid ratio = 0.1 mg/ 20 mL, natural pH, t = 360 min.

Voltage (V)	$q_{e,\ exp}$ (mg/g)	Pseudo-first order $q_t = q_e\ (1- \exp\ (-k_1 \cdot t))$				Pseudo-second order $q_t = t/((1/k_2 \cdot q_e^2)+(1/q_e) \cdot t)$			
		q_e (mg/g)	k_1 (min^{-1})	R^2	SEE	q_e (mg/g)	k_2 (g/mg·min)	R^2	SEE
0.8	0.500	0.622	0.005	0.968	0.035	0.893	$3.98 \cdot 10^{-3}$	0.972	0.032
1.0	1.050	1.486	0.004	0.992	0.041	2.374	$1.01 \cdot 10^{-3}$	0.990	0.044
1.2	1.690	1.808	0.006	0.995	0.047	2.520	$2.09 \cdot 10^{-3}$	0.998	0.030
1.3	1.400	1.667	0.005	0.996	0.035	2.428	$1.68 \cdot 10^{-3}$	0.997	0.034

ities estimated with the pseudo-first order kinetic model are very similar to the experimental data, the analogous values of the coefficients of determination and SEE prevent rigorous conclusions about a plausible adsorption mechanism. Considering the intraparticle diffusion coefficient determined by Eq. (6), the authors suggested the presence of a complex mechanism described by the nonlinear Sutherland model (Eq.7). As before, the statistical parameters showed a good fit, suggesting that the presence of an electric field can modify the adsorption mechanisms, leading to a more complex system. The energy consumption per unit removed mass estimated by the Eq. (3) followed the ascending order 1.2 V < 1.0 V < 1.3 V < 0.8 V, which is consistent with the adsorption capacities reported above (Table 4).

The adsorption capacity of the aerogel could decrease due to the saturation of the active sites by organic compounds from the wastewater. Although plausible reusability is one of the main criteria for the selection of long-term adsorbents, these recycling experiments allow the elucidation of the crucial role of the electrosorption mechanism in fluoxetine removal. After each adsorption run, the carbonaceous aerogel pellets were collected and immersed in acetonitrile for the desorption process. Then, the performance of the aerogel in the next cycle was evaluated. As shown in Fig. 4, the regenerated pellets retained around 98 % of their original adsorption capacities even after five successive cycles. In addition, these desorption experiments confirmed that the adsorbed mass on the carbon pellet corresponded to the complete removal of fluoxetine. From these results, the authors concluded that there is no electrochemical oxidation process and that the carbon aerogel pellets have excellent recycling capacity. In addition, the aerogel exhibited good stability, which was confirmed by the analysis of the morphological characteristics of aerogels after electrosorption under the field emission scanning electron microscope and energy-dispersive X-ray spectroscopy (FE-SEM/EDS) (Fig. 2b). As can be seen in Fig. 2a and b, the SEM images show a similar compact surface and the elemental composition of both aerogels content similar high levels of carbon, oxygen and metals such as iron and copper were detected, confirming that the aerogel keep its chemical composition after electrosorption.

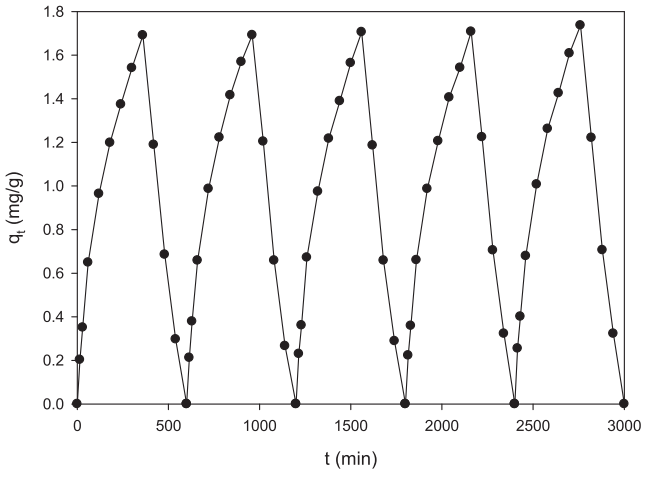

Fig. 4. Reusability capacity of the carbonaceous aerogel pellets after five consecutive cycles. Conditions: $[Fluoxetine]_0$ = 10 mg/L, pellet-liquid ratio = 0.1 mg/ 20 mL, natural pH, V = 1.2 V, t = 600 min/cycle. Data represent mean values with a standard deviation below 5 %.

3.5. Effect of wastewater matrix on the electrosorption of fluoxetine

After confirming the good performance of electrosorption in removing fluoxetine from synthetic water, the effect of water matrix was analysed using municipal wastewater spiked with the antidepressant. Considering typical drug concentrations in wastewater ranging from 0.1 to 200 μg/L, the municipal wastewater was fortified with 10 mg/L fluoxetine to achieve a concentration high enough for kinetic studies using conventional analytical techniques. As expected, pollutant removal was significantly lower than in the synthetic effluents due to the complexity of the water matrix (Table S2). The use of complex matrices negatively affects the effectiveness of the process, as relatively lower adsorption capacities are obtained compared to the synthetic wastewater (1.69 mg/g). In particular, the adsorption capacities decrease to about 1.1, 1.3 and 1.5 mg/g when raw wastewater, primary treatment wastewater and tertiary treatment wastewater were used as the water matrix.

The limitation of pharmaceutical removal by competitive adsorption may be caused by the presence of inorganic ions such as nitrate, nitrite and phosphates, as well as organic matter in the main solution. For this reason, the quantification of these inorganic ions in the main solution by chromatographic techniques allowed to determine their maximum contribution to the electroadsorptive process. After the electroadsoprtion treatment, a negligible ionic content was found in the solution, indicating a competitive adsorption process. These results are consistent with those of Pastushok et al. [35], who demonstrated the presence of some ions in the pores of the carbonaceous electrodes.

3.6. Electrosorption of a pharmaceutical mixture

Based on the previous results, the removal of a mixture of pharmaceutical compounds (10 mg/L each of antipyrine, sulfamethizole, and fluoxetine) collected in different water matrices from a municipal wastewater treatment plant was analysed by electrosorption. As described above, the minimum removal percentages are associated with adsoprtion of the pollutant on the carbon felt or anodic oxidation, demosntrating the electrochemical stability of these pollutants. These results are consistent with those of Bashkatova et al. [7], who analysed charge density distribution data over the antipyrine structure to determine the active atomic groups responsible for the total oxidation of the antidepressant antipyrine. They concluded that the oxidation of the molecular ring

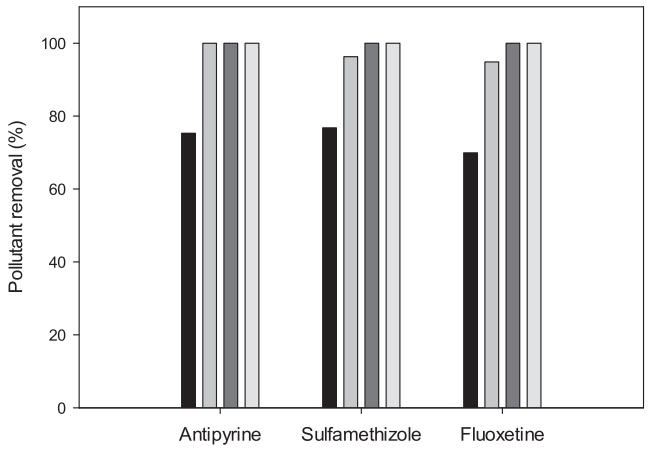

Fig. 5. Effect of the water matrices on the electrosorption of these ionisable drugs (antipyrine, sulfamethizole and fluoxetine). Conditions: $[Pollutant]_0$ = 10 mg/L, pellet-liquid ratio = 0.1 mg/ 20 mL, V = 1.2 V, natural pH, t = 600 min). Water matrices: Raw wastewater (black bar), effluent after primary treatment (medium grey bar), effluent from tertiary treatment (dark grey bar) and synthetic wastewater (light grey bar). Data represent mean values with a standard deviation below 5 %.

and the breakdown of the N—N bond occur at 1.35 V. After analysing the oxidation/reduction properties of antipyrine and sulfamethizole, the effect of the water matrix from the municipal treatment plant was evaluated by the electrosorption process. As can be seen in Fig. 5, the use of raw watewater as water matrix leads to the lower pollutant removal, which is due to the presence of organic matter in the fresh wastewater that causes the saturation of the adsorbent. As expected, the best results are obtained with the initial water, since the adsorption by the competition is minima, which ensures the potential use of this technology as an advanced treatment for the removal of pharmaceuticals. Moreover, these experimental values were compared with the adsorption capacity using a synthetic wastewater, obtaining similar results to those obtained with the municipal wastewater from tertiary treatment. As explained earlier, the application of the electric field to the aerogel pellets results in the formation of a 3D bipolar electrode; one side of each particle is positively charged, while the other side is negatively charged. This significantly increases the adsorption capacity of the pellets compared to the conventional adsorption described above.

The FTIR spectrum after electrosorption qualitatively confirmed the presence of these three ionisable compounds. As can be seen in Fig. S4b, the above-mentioned bands assigned to fluoxetine were again detected on the aerogel surface. For sulfamethizole, the bands associated with the symmetric and asymmetric stretching of aromatic —NH_2 are around 3500 cm^{-1}, while the peak at 3200 cm^{-1} corresponds to the stretching vibration of the S—N bond in SO_2NH. Two other peaks associated with the stretching and bending vibration of the O=S=O bond were observed at 1500 and 500 cm^{-1}, respectively, confirming the loading of sulfamethizole into the aerogel. In constrat, the overlap of the several bands in the FTIR spectrum complicates the detection of the antipyrine, whose main characteristic bands correspond to the symmetric and asymmetric stretching of the aromatic —NH_2 at 3400 cm^{-1} and the stretching vibration of the azomethine group around 1640 cm^{-1}.

As mentioned above, the kinetic studies were performed to analyse the plausible modifications of the controlled adsorption phase in the presence of an electric field in different water matrices. The experimental data were fitted to the pseudo-first and pseudo-second kinetic models and the estimated kinetic parameters are summarised in Table 5. As expected, considering previous results, these results do not shed light on the mechanism of electrosorption. Thus, the authors proposed a multi-mechanism driven by intraparticle diffusion followed by chemisorption, similar to the previous analysis. The experimental data were fitted to the Sutherland model, resulting in higher coefficients of determination and lower SEE and intraparticle diffusion coefficients estimated by Eq. (6), whose value around $3.6{\cdot}10^{-5}$ cm^2/s, confirmed intraparticle diffusion as rate-limiting step.

3.7. Microtox tests

The Microtox® toxicity test was reported as an adequate global indicator to evaluate the effectiveness of the process. The percentage of the bioluminescence inhibition expressed as the ratio of lost activity to remaining activity after 15-min exposure time was estimated using the Microtox OMNI software. The mixture of drugs (10 mg/L each of antipyrine, sulfamethizole, and fluoxetine) spiked in different water matrices was used as influent. The luminescence inihibition ratio before- and after-treatment was determined based on Microtox® test results according to the Eq. (8).

$$I = (1 - L_s/L_C) \cdot 100 \quad (8)$$

where I is the luminescence inhibition ratio (%) and Ls and Lc are the luminescence values of the sample and control after 15 min-exposure time.

After electrosorption, the luminescence inhibition estimated by Eq. (8) decreased by 79.8, 70.9 and 55.8 % compared to the polluted

Table 5
Pseudo-first and pseudo-second order kinetic parameters for electrosorption of these ionisable drugs (antipyrine, sulfamethizole and fluoxetine) on different water matrices. Conditions: $[Pollutant]_0$ = 10 mg/L, pellet-liquid ratio = 0.1 mg/ 20 mL, V = 1.2 V, natural pH, t = 600 min).

Water matrix	Pollutant	$q_{e,\,exp}$ (mg/g)	Pseudo-first order $q_t = q_e\,(1\text{- exp }(-k_1{\cdot}t))$				Pseudo-second order $q_t = t/((1/k_2{\cdot}q_e^2)+(1/q_e){\cdot}t)$			
			q_e (mg/g)	k_1 (min^{-1})	R^2	SEE	q_e (mg/g)	k_2 (g/mg·min)	R^2	SEE
Raw wastewater	**Antipyrine**	1.503	1.755	0.002	0.996	0.043	2.556	$6.46{\cdot}10^{-4}$	0.994	0.053
	Sulfamethizole	1.561	1.879	0.002	0.996	0.046	2.786	$5.22{\cdot}10^{-4}$	0.994	0.053
	Fluoxetine	1.341	1.652	0.002	0.993	0.054	2.494	$5.51{\cdot}10^{-4}$	0.989	0.064
Effluent after primary treatment	**Antipyrine**	1.954	2.350	0.002	0.997	0.048	3.467	$4.28{\cdot}10^{-4}$	0.996	0.058
	Sulfamethizole	1.918	2.271	0.002	0.997	0.046	3.316	$4.78{\cdot}10^{-4}$	0.996	0.057
	Fluoxetine	1.780	2.402	0.002	0.994	0.065	3.788	$2.71{\cdot}10^{-4}$	0.992	0.074
Effluent after tertiary treatment	**Antipyrine**	2.014	2.225	0.003	0.997	0.050	3.060	$2.27{\cdot}10^{-4}$	0.995	0.063
	Sulfamethizole	2.053	2.326	0.003	0.997	0.051	3.274	$5.94{\cdot}10^{-4}$	0.996	0.059
	Fluoxetine	1.934	2.407	0.002	0.996	0.059	3.625	$3.65{\cdot}10^{-4}$	0.994	0.069
Synthetic wastewater	**Antipyrine**	2.000	2.335	0.003	0.993	0.073	3.323	$6.60{\cdot}10^{-4}$	0.991	0.083
	Sulfamethizole	2.049	2.304	0.003	0.991	0.081	3.174	$8.40{\cdot}10^{-4}$	0.990	0.089
	Fluoxetine	1.948	2.337	0.003	0.993	0.073	3.406	$5.74{\cdot}10^{-4}$	0.989	0.087

influent for the raw wastewater and the effluents from the primary and tertiary treatment as water matrix, respectively. As expected, the application of remediation technologies for municipal wastewater efficiently reduces the toxic load of the effluent [3]. Nonetheless, electrosorption process allows the removal of these pharmaceuticals without toxic effects at the highest evaluated concentrations. Regardless the decrease in COD values (Table S2) after electrosorption process does not correlate with the toxicity of the effluents, since the effluent are intrinsically variable as previously shown by Guerra [17] and Araújo et al. [3].

4. Conclusions

Three ionisable pharmaceuticals (antipyrine, sulfamethizole, and fluoxetine) were tested as target pollutants to analyse the potential use of carbonaceous aerogel pellets as adsorbents. At a circumneutral pH, the surface of the aerogel is positively charged, which promotes the adsorption of neutral/anionic pollutants such as sulfamethizole and antipyrine. Nevertheless, under the same conditions, negligible removal of fluoxetine, an example of a cationic pollutant, was achieved. Consequently, the authors proposed the application of an electric field as a functional tool to improve the poor adsorption affinity of the pollutant. The effect of the applied voltage was studied in the range of 0.8 and 1.3 V, with the maximum removal achieved at 1.2 V. Under these conditions, the carbonaceous aerogels became a porous polarised 3D material. After demonstrating the excellent performance of the aerogel, the influence of the water matrix and additional impurities in the solution was analysed, revealing the presence of other competing molecules that led to the saturation of the adsorbent and compromised the effectiveness of the process. Finally, Microtox® tests were able to confirm the suitability of these carbonaceous aerogel pellets for the removal of ionisable pharmaceuticals.

The authors declare that do not have known any financial and personal relationships that could inappropriately influence/bias the work reported in this paper.

CRediT authorship contribution statement

A. Puga: Investigation, Data curation, Formal analysis. **J. Meijide:** Writing – original draft, Writing – review & editing. **M. Pazos:** Resources, Funding acquisition, Project administration, Writing – review & editing. **E. Rosales:** Conceptualization, Validation, Writing – review & editing. **M.A. Sanromán:** Conceptualization, Resources, Funding acquisition, Project administration, Writing – review & editing.

Declaration of Competing Interest

The authors declare that they have no known competing financial interests or personal relationships that could have appeared to influence the work reported in this paper.

Acknowledgements

This research has been financially supported Project PDC2021-121394-I00 funded by MCIN / AEI /10.13039/501100011033 and by the European Union Next Generation EU / PRTR, PID2020-113667 GB-I00 funded by MCIN / AEI /10.13039/501100011033, and Xunta de Galicia and ERDF (ED431C 2021-43). The authors are grateful to the Xunta de Galicia for the financial support of Jessica Meijide under her postdoctoral fellowship (ED481B 2018/096), and to the Universidade de Vigo/Consorcio Interuniversitario de Galicia (CISUG) for open access charge.

Appendix A. Supplementary material

Supplementary data to this article can be found online at https://doi.org/10.1016/j.molliq.2022.120269.

References

[1] O. Abbas, G. Compère, Y. Larondelle, D. Pompeu, H. Rogez, V. Baeten, Phenolic compound explorer: A mid-infrared spectroscopy database, Vib. Spectrosc. 92 (2017) 111–118, https://doi.org/10.1016/J.VIBSPEC.2017.05.008.
[2] M.B. Ahmed, J.L. Zhou, H.H. Ngo, W. Guo, Adsorptive removal of antibiotics from water and wastewater: Progress and challenges, Sci. Total Environ. 532 (2015) 112–126, https://doi.org/10.1016/J.SCITOTENV.2015.05.130.
[3] C.V.M. Araújo, R.B. Nascimento, C.A. Oliveira, U.J. Strotmann, E.M. da Silva, The use of Microtox® to assess toxicity removal of industrial effluents from the industrial district of Camaçari (BA, Brazil), Chemosphere 58 (9) (2005) 1277–1281.
[4] J.A. Arcibar-Orozco, J.R. Rangel-Mendez, T.J. Bandosz, Reactive adsorption of SO_2 on activated carbons with deposited iron nanoparticles, J. Hazard. Mater. 246–247 (2013) 300–309, https://doi.org/10.1016/J.JHAZMAT.2012.12.001.
[5] V.P. Barba, B. Selvaratnam, P. Thangarasu, R.T. Koodali, How porous periodicity of mesoporous materials like TiO2-SBA-15-10 encourages photocatalytic degradation of rhodamine B: A comparative study with aperiodic TiO_2-SiO_2-aerogel-10, J. Nanopart. Res. 23 (2021) 32, https://doi.org/10.1007/s11051-021-05148-x.
[6] L.P. Bakos, J. Mensah, K. László, T. Igricz, I.M. Szilágyi, Preparation and characterization of a nitrogen-doped mesoporous carbon aerogel and its polymer precursor, J. Therm. Anal. Calorim. 134 (2) (2018) 933–939, https://doi.org/10.1007/s10973-018-7318-4.
[7] N.V. Bashkatova, E.I. Korotkova, Y.A. Karbainov, A.Y. Yagovkin, A.A. Bakibaev, Electrochemical, quantum-chemical and antioxidant properties of antipyrine and its derivatives, J. Pharm. Biomed. Anal. 37 (5) (2005) 1143–1147.
[8] H.P. Boehm, Chemical Identification of Surface Groups, Adv. Catal. 16 (1966) 179–274, https://doi.org/10.1016/S0360-0564(08)60354-5.
[9] B.S. Chittoo, C. Sutherland, Adsorption of phosphorus using water treatment sludge, J. Appl. Sci. 14 (24) (2014) 3455–3463, https://doi.org/10.3923/jas.2014.3455.3463.
[10] J.G.D.R.d. Costa, J.M. Costa, A.F.d. Almeida Neto, Recent advances and future applications in electro-adsorption technology: An updated review, J. Environ. Chem. Eng. 9 (6) (2021) 106355.
[11] G. Divyapriya, J. Mohanalakshmi, K.V. kumar, I.M. Nambi, Electro-enhanced adsorptive removal of ciprofloxacin from aqueous solution on graphite felt, J. Environ. Chem. Eng. 8 (5) (2020) 104299.
[12] G. Divyapriya, R. Srinivasan, I.M. Nambi, J. Senthilnathan, Highly active and stable ferrocene functionalized graphene encapsulated carbon felt array - A novel rotating disc electrode for electro-Fenton oxidation of pharmaceutical compounds, Electrochim. Acta 283 (2018) 858–870, https://doi.org/10.1016/J.ELECTACTA.2018.06.186.
[13] N. Fiol, I. Villaescusa, Determination of sorbent point zero charge: usefulness in sorption studies, Environ. Chem. Lett. 7 (1) (2009) 79–84, https://doi.org/10.1007/s10311-008-0139-0.
[14] S.L. Goertzen, K.D. Thériault, A.M. Oickle, A.C. Tarasuk, H.A. Andreas, Standardization of the Boehm titration. Part I. CO_2 expulsion and endpoint determination, Carbon N. Y. 48 (4) (2010) 1252–1261.
[15] O.I. González Peña, M.Á. López Zavala, H. Cabral Ruelas, Pharmaceuticals market, consumption trends and disease incidence are not driving the pharmaceutical research on water and wastewater, Int. J. Environ. Res. Public Health 18 (2021) 2532, https://doi.org/10.3390/ijerph18052532.
[16] J.A.O. Granados, P. Thangarasu, N. Singh, J.M. Vázquez-Ramos, Tetracycline and its quantum dots for recognition of Al^{3+} and application in milk developing cells bio-imaging, Food Chem. 278 (2019) 523–532, https://doi.org/10.1016/j.foodchem.2018.11.086.
[17] R. Guerra, Ecotoxicological and chemical evaluation of phenolic compounds in industrial effluents, Chemosphere 44 (8) (2001) 1737–1747, https://doi.org/10.1016/S0045-6535(00)00562-2.
[18] Q. Huang, S. Deng, D. Shan, Y. Wang, B. Wang, J. Huang, G. Yu, Enhanced adsorption of diclofenac sodium on the carbon nanotubes-polytetrafluorethylene electrode and subsequent degradation by electro-peroxone treatment, J. Colloid Interface Sci. 488 (2017) 142–148, https://doi.org/10.1016/J.JCIS.2016.11.001.
[19] C.A. Huerta-Aguilar, Y.S. García Gutiérrez, P. Thangarasu, Crystal plane directed interaction of TiO_2 [1 0 1] with AgNPs [1 1 1] silver nanoparticles enhancing solar light induced photo-catalytic oxidation of ciprofloxacin: Experimental and theoretical studies, Chem. Eng. J. 394 (2020) 124286, https://doi.org/10.1016/J.CEJ.2020.124286.
[20] A. Langdon, N. Crook, G. Dantas, The effects of antibiotics on the microbiome throughout development and alternative approaches for therapeutic modulation, Genome Med. 8 (2016) 39, https://doi.org/10.1186/s13073-016-0294-z.
[21] W. Lertpaitoonpan, S.K. Ong, T.B. Moorman, Effect of organic carbon and pH on soil sorption of sulfamethazine, Chemosphere 76 (4) (2009) 558–564.
[22] H. Li, H. Yang, J. Cheng, C. Hu, Z. Yang, C. Wu, Three-dimensional particle electrode system treatment of organic wastewater: A general review based on patents, J. Clean. Prod. 308 (2021) 127324.

[23] R. Li, Z. Wang, J. Guo, Y. Li, H. Zhang, J. Zhu, X. Xie, Enhanced adsorption of ciprofloxacin by KOH modified biochar derived from potato stems and leaves, Water Sci. Technol. 77 (2018) 1127–1136, https://doi.org/10.2166/wst.2017.636.
[24] M.A. Lillo-Ródenas, D. Cazorla-Amorós, A. Linares-Solano, Understanding chemical reactions between carbons and NaOH and KOH: An insight into the chemical activation mechanism, Carbon N. Y. 41 (2) (2003) 267–275, https://doi.org/10.1016/S0008-6223(02)00279-8.
[25] X. Liu, J. Wang, Electro-adsorption characteristics and mechanism of Sr2+ ions by capacitive deionization and CFD analysis study, Prog. Nucl. Energy 133 (2021) 103628.
[26] M.I. López-Cázares, E.D. Isaacs-Páez, J. Ascacio-Valdés, C.N. Aguilar-González, J. R. Rangel-Mendez, L.F. Chazaro-Ruiz, Electro-assisted naproxen adsorption followed by its electrodegradation and simultaneous electroreactivation of the activated carbon electrode, Sep. Purif. Technol. 258 (2021) 118030.
[27] Y. Lv, Z. Liang, Y. Li, Y. Chen, K. Liu, G. Yang, Y. Liu, C. Lin, X. Ye, Y. Shi, M. Liu, Efficient adsorption of diclofenac sodium in water by a novel functionalized cellulose aerogel, Environ. Res. 194 (2021) 110652, https://doi.org/10.1016/j.envres.2020.110652.
[28] C. Macias, G. Rasines, T. García, M. Zafra, P. Lavela, J. Tirado, C. Ania, Synthesis of Porous and Mechanically Compliant Carbon Aerogels Using Conductive and Structural Additives, Gels 2 (1) (2016) 4, https://doi.org/10.3390/gels2010004.
[29] J. Meijide, P.S.M. Dunlop, M. Pazos, M.A. Sanromán, Heterogeneous electro-fenton as "Green" technology for pharmaceutical removal: A review, Catalysts 11 (2021) 1–22, https://doi.org/10.3390/catal11010085.
[30] J. Meijide, S. Rodríguez, M.A. Sanromán, M. Pazos, Comprehensive solution for acetamiprid degradation: Combined electro-Fenton and adsorption process, J. Electroanal. Chem. 808 (2018) 446–454, https://doi.org/10.1016/j.jelechem.2017.05.012.
[31] S.E. Muehlemann, L. Huber, S. Zhao, S.K. Matam, M.M. Koebel, Facile synthesis of resorcinol-melamine-formaldehyde based carbon xerogel, Mater. Today Proc. 5 (2018) 13776–13784, https://doi.org/10.1016/j.matpr.2018.02.018.
[32] J. Narayanan, J.G. Hernández, I.I. Padilla-Martínez, P. Thangarasu, S.E. Santos Garay, C.B. Palacios Cabrera, A.J. Santiago Cuevas, Geometry influenced adsorption of fluoxetine over the surface of $RuFeO_3$ and $CeFeO_3$ nanoparticles: Kinetics and thermodynamic studies, Ceram. Int. 47 (14) (2021) 20544–20561, https://doi.org/10.1016/j.ceramint.2021.04.064.
[33] L. Nielsen, T.J. Bandosz, Analysis of the competitive adsorption of pharmaceuticals on waste derived materials, Chem. Eng. J. 287 (2016) 139–147, https://doi.org/10.1016/J.CEJ.2015.11.016.
[34] G.-F. Norra, J. Radjenovic, Removal of persistent organic contaminants from wastewater using a hybrid electrochemical-granular activated carbon (GAC) system, J. Hazard. Mater. 415 (2021) 125557.
[35] O. Pastushok, D.L. Ramasamy, M. Sillanpää, E. Repo, Enhanced ammonium removal and recovery from municipal wastewater by asymmetric CDI cell equipped with oxygen functionalized carbon electrode, Sep. Purif. Technol. 274 (2021) 119064.
[36] A.L. Patterson, The Scherrer Formula for X-Ray Particle Size Determination, Phys. Rev. 56 (10) (1939) 978–982, https://doi.org/10.1103/PhysRev.56.978.
[37] W. Peng, G. Han, Y. Huang, Y. Cao, S. Song, Insight the effect of crystallinity of natural graphite on the electrochemical performance of reduced graphene oxide, Results Phys. 11 (2018) 131–137, https://doi.org/10.1016/J.RINP.2018.08.055.
[38] A. Pholosi, E.B. Naidoo, A.E. Ofomaja, Intraparticle diffusion of Cr(VI) through biomass and magnetite coated biomass: A comparative kinetic and diffusion study, South African J. Chem. Eng. 32 (2020) 39–55, https://doi.org/10.1016/J.SAJCE.2020.01.005.
[39] M.A. Pimenta, G. Dresselhaus, M.S. Dresselhaus, L.G. Cançado, A. Jorio, R. Saito, Studying disorder in graphite-based systems by Raman spectroscopy, Phys. Chem. Chem. Phys. 9 (11) (2007) 1276–1290, https://doi.org/10.1039/B613962K.
[40] A. Puga, M.M. Moreira, M. Pazos, S.A. Figueiredo, M.Á. Sanromán, C. Delerue-Matos, E. Rosales, Continuous adsorption studies of pharmaceuticals in multicomponent mixtures by agroforestry biochar, J. Environ. Chem. Eng. 10 (1) (2022) 106977.
[41] A. Puga, M. Pazos, E. Rosales, M.A. Sanromán, Electro-reversible adsorption as a versatile tool for the removal of diclofenac from wastewater, Chemosphere 280 (2021) 130778.
[42] A. Puga, E. Rosales, M.A. Sanromán, M. Pazos, Environmental application of monolithic carbonaceous aerogels for the removal of emerging pollutants, Chemosphere 248 (2020) 125995.
[43] D.L.O. Ramos, J.M. Freitas, R.A.A. Munoz, E.M. Richter, Simple and rapid voltammetric method for the detection of the synthetic adulterant fluoxetine in weight loss products, J. Electroanal. Chem. 882 (2021) 115028.
[44] G. Rasines, P. Lavela, C. Macías, M.C. Zafra, J.L. Tirado, C.O. Ania, On the use of carbon black loaded nitrogen-doped carbon aerogel for the electrosorption of sodium chloride from saline water, Electrochim. Acta 170 (2015) 154–163, https://doi.org/10.1016/J.ELECTACTA.2015.04.137.
[45] E. Rosales, J. Meijide, T. Tavares, M. Pazos, M.A. Sanromán, Grapefruit peelings as a promising biosorbent for the removal of leather dyes and hexavalent chromium, Process Saf. Environ. Prot. 101 (2016) 61–71, https://doi.org/10.1016/J.PSEP.2016.03.006.
[46] M.N. Sepehr, A. Amrane, K.A. Karimaian, M. Zarrabi, H.R. Ghaffari, Potential of waste pumice and surface modified pumice for hexavalent chromium removal: Characterization, equilibrium, thermodynamic and kinetic study, J. Taiwan Inst. Chem. Eng. 45 (2) (2014) 635–647.
[47] J.C. Serna-Carrizales, V.H. Collins-Martínez, E. Flórez, C.F.A. Gomez-Duran, G. Palestino, R. Ocampo-Pérez, Adsorption of sulfamethoxazole, sulfadiazine and sulfametazine in single and ternary systems on activated carbon. Experimental and DFT computations, J. Mol. Liq. 324 (2021) 114740.
[48] J. Shin, J. Kwak, Y.-G. Lee, S. Kim, M. Choi, S. Bae, S.-H. Lee, Y. Park, K. Chon, Competitive adsorption of pharmaceuticals in lake water and wastewater effluent by pristine and NaOH-activated biochars from spent coffee wastes: Contribution of hydrophobic and π-π interactions, Environ. Pollut. 270 (2021) 116244.
[49] X. Tan, Y. Liu, G. Zeng, X. Wang, X. Hu, Y. Gu, Z. Yang, Application of biochar for the removal of pollutants from aqueous solutions, Chemosphere 125 (2015) 70–85, https://doi.org/10.1016/J.CHEMOSPHERE.2014.12.058.
[50] S. Tang, M. Zhao, D. Yuan, X. Li, Z. Wang, X. Zhang, T. Jiao, J. Ke, Fe3O4 nanoparticles three-dimensional electro-peroxydisulfate for improving tetracycline degradation, Chemosphere 268 (2021) 129315.
[51] E. Tecuapa-Flores, J.G. Hernández, P. Roquero-Tejeda, J.A. Arenas-Alatorre, P. Thangarasu, Rapid electrochemical recognition of trimethoprim in human urine samples using new modified electrodes (CPE/Ag/Au NPs) analysing tunable electrode properties: Experimental and theoretical studies, Analyst 146 (24) (2021) 7653–7669, https://doi.org/10.1039/d1an01408k.
[52] M. Thommes, K. Kaneko, A.V. Neimark, J.P. Olivier, F. Rodriguez-Reinoso, J. Rouquerol, K.S.W. Sing, Physisorption of gases, with special reference to the evaluation of surface area and pore size distribution (IUPAC Technical Report), Pure Appl. Chem. 87 (2015) 1051–1069, https://doi.org/10.1515/pac-2014-1117.
[53] P. Veselá, V. Slovák, Monitoring of N-doped organic xerogels pyrolysis by TG–MS, J. Therm. Anal. Calorim. 113 (1) (2013) 209–217, https://doi.org/10.1007/s10973-012-2923-0.
[54] S. Wang, X. Li, H. Zhao, X. Quan, S. Chen, H. Yu, Enhanced adsorption of ionizable antibiotics on activated carbon fiber under electrochemical assistance in continuous-flow modes, Water Res. 134 (2018) 162–169, https://doi.org/10.1016/J.WATRES.2018.01.068.
[55] Y. Wang, W.B. Jiao, J.T. Wang, G.F. Liu, H.L. Cao, J. Lü, Amino-functionalized biomass-derived porous carbons with enhanced aqueous adsorption affinity and sensitivity of sulfonamide antibiotics, Bioresour. Technol. 277 (2019) 128–135, https://doi.org/10.1016/J.BIORTECH.2019.01.033.
[56] A. Xie, J. Dai, X. Chen, P. Ma, J. He, C. Li, Z. Zhou, Y. Yan, Ultrahigh adsorption of typical antibiotics onto novel hierarchical porous carbons derived from renewable lignin via halloysite nanotubes-template and in-situ activation, Chem. Eng. J. 304 (2016) 609–620, https://doi.org/10.1016/J.CEJ.2016.06.138.
[57] Y. Xiong, J. Zhao, L. Li, Y. Wang, X. Dai, F. Yu, J. Ma, Interfacial interaction between micro/nanoplastics and typical PPCPs and nanoplastics removal via electrosorption from an aqueous solution, Water Res. 184 (2020) 116100.
[58] W. Yang, H. Han, M. Zhou, J. Yang, Simultaneous electricity generation and tetracycline removal in continuous flow electrosorption driven by microbial fuel cells, RSC Adv. 5 (61) (2015) 49513–49520, https://doi.org/10.1039/C5RA05545H.
[59] M.C. Zafra, P. Lavela, C. Macías, G. Rasines, J.L. Tirado, Electrosorption of environmental concerning anions on a highly porous carbon aerogel, J. Electroanal. Chem. 708 (2013) 80–86, https://doi.org/10.1016/J.JELECHEM.2013.09.020.
[60] M.C. Zafra, P. Lavela, G. Rasines, C. Macías, J.L. Tirado, C.O. Ania, A novel method for metal oxide deposition on carbon aerogels with potential application in capacitive deionization of saline water, Electrochim. Acta 135 (2014) 208–216, https://doi.org/10.1016/J.ELECTACTA.2014.04.182.
[61] C. Zhang, Y. Jiang, Y. Li, Z. Hu, L. Zhou, M. Zhou, Three-dimensional electrochemical process for wastewater treatment: A general review, Chem. Eng. J. 228 (2013) 455–467, https://doi.org/10.1016/J.CEJ.2013.05.033.
[62] H. Zhou, S. Xu, H. Su, M. Wang, W. Qiao, L. Ling, D. Long, Facile preparation and ultra-microporous structure of melamine–resorcinol–formaldehyde polymeric microspheres, Chem. Commun. 49 (2013) 3763–3765, https://doi.org/10.1039/C3CC41109E.